Back Cover: Spontaneous Stepwise Self-Assembly of a Polyoxometalate–Organic Hybrid into Catalytically Active One-Dimensional Anisotropic Structures (Chem. Eur. J. 31/2014)

ARTICLE *in* CHEMISTRY - A EUROPEAN JOURNAL · JULY 2014

Impact Factor: 5.73 · DOI: 10.1002/chem.201402974

ChemPubSoc Europe

DOI: 10.1002/chem.201402974

CHEMISTRY A European Journal Full Paper

Organic–Inorganic Hybrids

Spontaneous Stepwise Self-Assembly of a Polyoxometalate–Organic Hybrid into Catalytically Active One-Dimensional Anisotropic Structures

Panchao Yin,[a, b] Aruuhan Bayaguud,[c] Peng Cheng,[b] Fadi Haso,[a, b] Lang Hu,[a] Joy Wang,[b] Dmitri Vezenov,[b] Randall E. Winans,[d] Jian Hao,[c] Tao Li,*[d] Yongge Wei,*[c] and Tianbo Liu*[a, b]

Abstract: An inorganic–organic hybrid surfactant with a hexavanadate cluster as the polar head group was designed and observed to assemble into micelle structures, which further spontaneously coagulate into a 1D anisotropic structure in aqueous solutions. Such a hierarchical self-assembly process is driven by the cooperation of varied noncovalent interactions, including hydrophobic, electrostatic, and hydrogen-bonding interactions. The hydrophobic interaction drives the quick formation of the micelle structure; electrostatic interactions involving counterions leads to the further coagulation of the micelles into larger assemblies. This process is similar to the crystallization process, but the specific counterions and the directional hydrogen bonding lead to the 1D growth of the final assemblies. Since most of the hexavanadates are exposed to the surface, the 1D assembly with nanoscale thickness is a highly efficient heterogeneous catalyst for the oxidation of organic sulfides with appreciable recyclability.

Introduction

The self-assembly of molecules, nanoparticles, and colloids into well-defined micro- and macrostructures represents one of the key bottom-up protocols in building up artificial devices and basic functional units of virus and cell.[1] The self-assembly strategies give us the ability to meet the requirements of both morphology and functionality in materials design across multiple-length scales, while starting from relatively simple building units.[1c,2] Despite the great achievements scientists have been making in supramolecular chemistry and materials science, a thorough understanding of the comprehensive roles of noncovalent interactions, including electrostatic interactions, hydrogen bonding, hydrophobic interactions, and aromatic stacking interactions, in one self-assembly process is challenging, but critical for the design of the building units and programming the self-assembly process.[3] The emergence of multifunctional building units and the need of assemblies with complicated structures has prompted researchers to focus on the rational design of the noncovalent interactions to work cooperatively in the self-assembly process.[3b,c] A detailed study of the self-assembly mechanism (e.g., kinetics and intermediate state) resulting from the cooperative work of various noncovalent interactions is instructive for establishing the design rules for synthesizing starting units of functional assemblies.[4]

Polyoxometalates (POMs) are a large group of nanoscopic metal oxide clusters with well-defined molecular structures and wide applications in catalytic, photoelectronic, and magnetic materials; medicine; and nanoscale building scaffolds.[5] Many POMs are highly negatively charged and their surfaces are abundant in oxo, hydroxo, or bound water ligands, providing opportunities for intermolecular electrostatic and hydrogen-bonding interactions.[6] Meanwhile, covalently grafting organic functional groups onto POM surfaces has been developed rapidly in recent years as the obtained novel amphiphilic inorganic–organic hybrid materials can expand the compatibility of hydrophilic POMs in organic media.[7] On the other hand, the processing of the POMs into nanoscaled materials could enhance their heterogeneous catalytic activity and build multiresponsive and/or bio/photoelectronic-active devices.[8] Herein, we report the unique spontaneous self-assembly process of long-alkyl-chain-functionalized POM hybrid molecules into a 1D nanobelt structure, cooperatively driven by hydrophobic,

[a] Dr. P. Yin, F. Haso, L. Hu, Prof. Dr. T. Liu
Department of Polymer Science, The University of Akron
Akron, Ohio 44325-3909 (USA)
Phone: (+1) 3309723496
E-mail: tliu@uakron.edu

[b] Dr. P. Yin, P. Cheng, F. Haso, J. Wang, Prof. Dr. D. Vezenov, Prof. Dr. T. Liu
Department of Chemistry, Lehigh University
Bethlehem, Pennsylvania 18015 (USA)

[c] A. Bayaguud, Dr. J. Hao, Prof. Dr. Y. Wei
Department of Chemistry, Tsinghua University
Beijing 100084 (P. R. China)
E-mail: yonggewei@mail.tsinghua.edu.cn

[d] Dr. R. E. Winans, Dr. T. Li
X-ray Science Division, Advanced Photon Source
Argonne National Laboratory, Argonne, Illinois 60439 (USA)
E-mail: taoli@aps.anl.gov

Supporting information for this article is available on the WWW under http://dx.doi.org/10.1002/chem.201402974.

hydrogen-bonding, and electrostatic interactions, with the directional hydrogen bonding playing a key role for the anisotropic features of the assemblies. Suggested by time-resolved small-angle X-ray scattering (SAXS) and TEM studies on their aqueous solutions, the hybrid molecules quickly assemble into micelle structures, followed by a slowly coagulation process of the micelles into nanobelt structures. Moreover, due to its nanoscale thickness (ca. 20 nm), the resulting 1D assembly structure has an extremely high surface area, demonstrating its potential application as highly efficient heterogeneous catalyst in oxidation desulfurization reactions.

Results and Discussion

Molecular structure of the hybrid surfactant

The molecular structure of the hybrid anion $[V_6O_{13}(OCH_2)_3CNH_2(OCH_2)_3CNHCH_2C_6H_4COOC_{16}H_{33}]^{2-}$ ($\mathbf{1}^{2-}$) is a typical single-tailed surfactant with the hexavanadate cluster as the polar head group (Figure 1a and Supporting Information).[9] The surfactant was synthesized through the so-called post-functionalization protocol by a reaction of a hexavanadate unit containing amino groups with a chloro-functionalized alkyl tail in stoichiometric ratio (see Experimental Section and Supporting Information).[7c] The large super-octahedron-shaped hexavanadate polar head group is about 0.8 nm in size with a charge of -2.[9] Its surface is composed of terminal oxo ($V{=}O_t$) and μ_2-bridge oxo ligands ($V\text{-}O_b\text{-}V$), providing multiple hydrogen-bond-acceptor positions. Two amine groups are incorporated into the organic fragments of **1**, providing potential hydrogen-bond donors. Single-crystal X-ray diffraction analysis of $TBA_2{\cdot}\mathbf{1}$ (TBA, tetrabutyl ammonium) indicates that the hybrid molecule links to each of two neighboring clusters with double N–H···O hydrogen bonds to form 1D chain structures (Figure 1a). Mediated by the bulky TBA^+ ions, the chains of hexavanadate clusters are aligned and packed into the (001) lattice plane (Figure 1b). The zig-zag-shaped long alkyl chains of the hybrids pack together to fill the space between the lattice planes (Figure 1c).

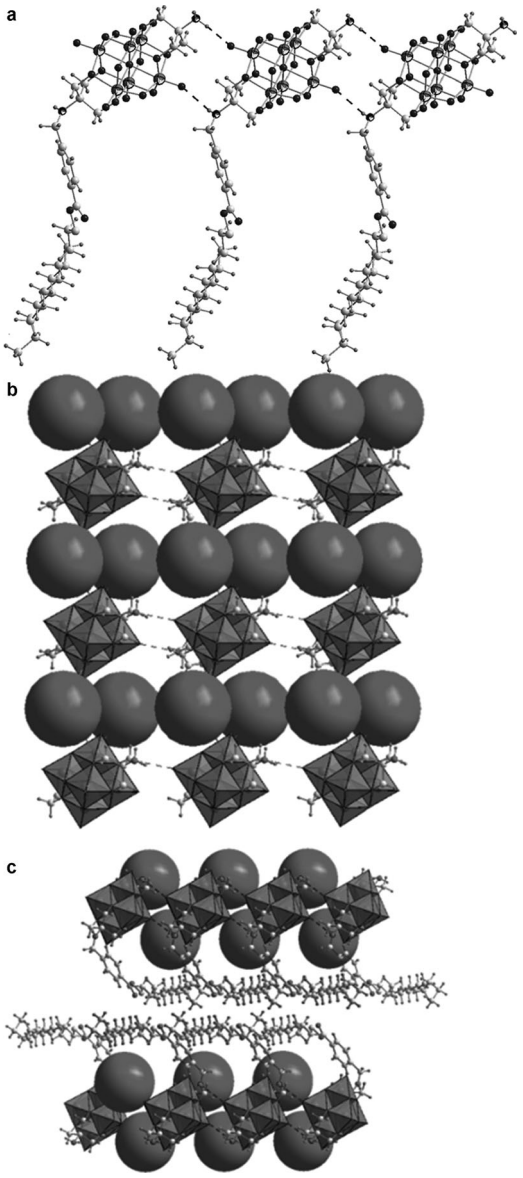

Figure 1. a) Hydrogen bonding between hexavanadate head groups of the hybrid molecules; atom code: light grey sphere, C; small dark sphere, H; dark sphere, O; large octant sphere, V; small octant sphere, N. b) Packing of hybrid molecules and their counterions, TBA^+ in lattice plane (001). c) Packing of (001) plane through alkyl chain interaction. Color code: grey sphereT-BA^+; grey octahedron, VO_6.

Formation and characterization of the 1D anisotropic assemblies

As a typical preparation procedure for the nanostructures, $H_2{\cdot}\mathbf{1}$ ($\mathbf{1}^{2-}$ with protons as counterions, 2.5 mg mL^{-1}) was dissolved in aqueous KOH solution (pH ~13.3) without any external stimulus. Complex $H_2{\cdot}\mathbf{1}$ was obtained by replacing the TBA^+ ions of $TBA_2{\cdot}\mathbf{1}$ with protons through a biphasic ion exchange technology (see Experimental Section and Supporting Information). Complex $H_2{\cdot}\mathbf{1}$ can be temporarily dissolved in aqueous KOH solution, driven by the acid–base reaction that increases the effective charge on the hexavanadates. The freshly obtained KOH solution of $H_2{\cdot}\mathbf{1}$ is clear and does not contain large assemblies right after the preparation, suggested by its low scattered intensity at 90° from static light scattering (SLS) studies (ca. 100 kcps; scattered intensity for benzene, 113 kcps). However, the solution became cloudy several hours after the preparation (Figure S1 in Supporting Information). One-dimensional aggregates with 100–300 μm in length dispersed in the solution were easily observed under optical microscope (Figure 2a). SEM and TEM results suggest that these aggregates are uniform 1D nanobelts with thickness and width at nanometer scale, while their lengths are at micrometer scale (Figure 2b and c). Atomic force microscopy (AFM) results confirm the belt shape of the aggregates in solution and are able to accurately determine the thickness of the nanobelts as about 20 nm (Figure 2d, e, and f). High-resolution TEM studies reveal the layered structures and the pattern packed by the polar head groups of surfactants on the nanobelt surface, suggesting a typical multilayer model (Figure 3 and 4b). There is no evi-

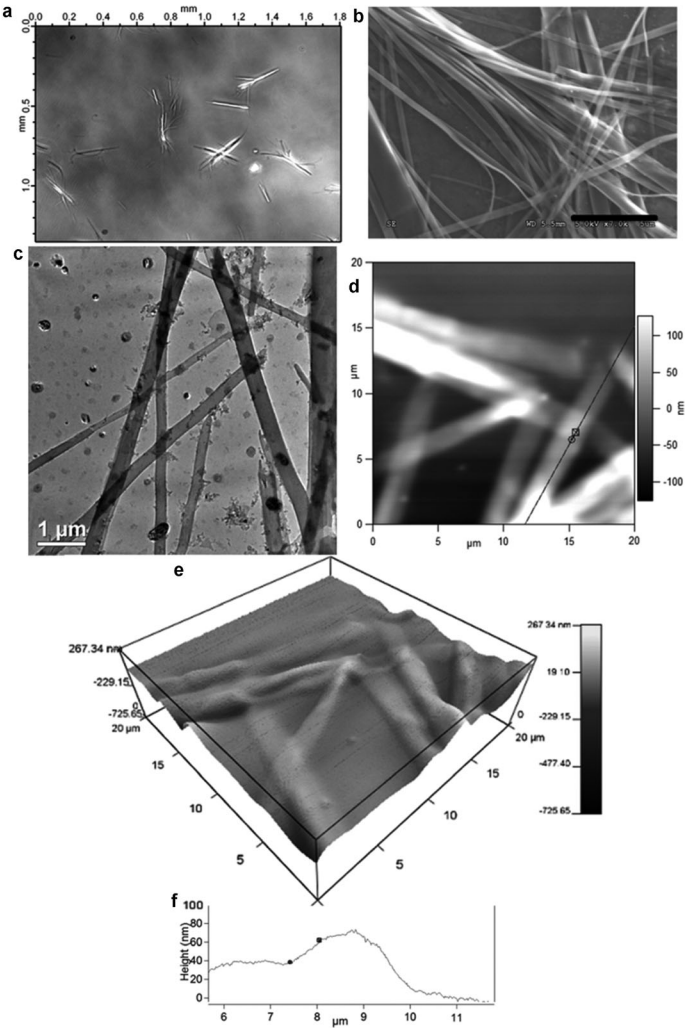

Figure 2. a) Optical microscopy images of the aggregates in mother liquor. b) SEM image of 1D anisotropic atructures (scale bar, 5 μm). c) TEM image of assembly structures. d) and e) AFM images of 1D anisotropic structures obtained under liquid. f) Height profile across the nanobelt taken along the selected line in d).

dent morphological change of the nanobelts in their mother liquors for at least two weeks according to the SEM studies, confirming their thermodynamic stability as the final assemblies (Figure S2 in Supporting Information). Additionally, FT-IR and ^{1}H NMR measurements were applied to confirm the stability of hybrid surfactant during the above preparation process of nanobelt structures, ruling out the possibility that the decomposition of the hybrid surfactant leads to the formation of nanobelts (see Supporting Information). The above crystal structural analysis suggests that the bulky TBA^+ ions strongly mediate the interlayer attraction, which is responsible for the obtaining of millimeter-scale needle-like single crystals of TBA_2·**1**. However, K^+ does not favor the growth of the assemblies along the *z*-direction, which therefore contributes to the nanoscaled thickness of the nanobelt structures of H_2·**1** in aqueous KOH solutions.

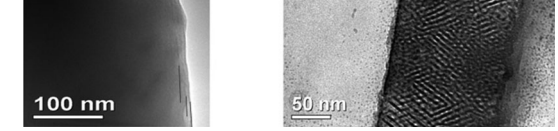

Figure 3. a) TEM image of the multilayer structure (inset, zoom in image of the layers; the three grey lines highlight the boundaries between the layers). b) TEM image of the pattern on the surface of the 1D anisotropic structures.

SAXS and TEM studies on the sequence of self-assembly of H_2·1 in KOH solution

Time-resolved SAXS and TEM studies indicate that, after the dissolution in KOH aqueous solution, the hybrid molecules firstly self-assemble into micelles, which further coagulate into nanobelt structures. SAXS measurements of the freshly prepared H_2·**1** solution with KOH (pH ~13.3) show a typical curve of core–shell structures with a total radius, core radius, and shell thickness of 4.2, 2.5, and 1.7 nm, respectively (Figure 4a).[10] The core–shell structure is consistent with the model of flower-like micelles formed by the hybrids, which is confirmed by the TEM studies of freshly prepared H_2·**1** solution (Figure 5a). The SAXS curve of the solution containing the assembled structures shows a sharp peak at $q = 0.202$ Å^{-1} ($d = 2\pi/q = 3.11$ nm), possibly corresponding to the interlayer distance of the lamellar packing of the hybrids (the length of single hybrid is 3.30 nm) (Figure 4b).[11] Time-resolved SAXS studies on the freshly prepared solution indicate that this sharp peak appeared and grew with time, while at the same time the characteristic oscillation curve for the micelles became weaker and completely disappeared after 680 min (Figure 4c). Detailed SAXS kinetic study data is summarized in Figure 4d by plotting the intensity of the sharp peak ($q = 0.202$ Å^{-1}) due to the nanobelt and the intensity of micelle curve versus time. Both plots show typical sigmoidal shape, suggesting a slow initial coagulation of micelle structures at the beginning of the self-assembly process.[12] During the self-assembly process, the micelles coagulate first and form primary layer structures at a 60 min lag phase, as suggested by the TEM studies (Figure 5b and 5c). This is typical for some step-wise association processes as the growth of the aggregates gradually accelerates the further aggregation.[13]

Effect of pH and counterions on the coagulation of micelles to give assembly structures

The formation of the assembly structures in the hybrid solutions with different pHs or different types of counterions has been explored by means of SEM and SAXS measurements. The

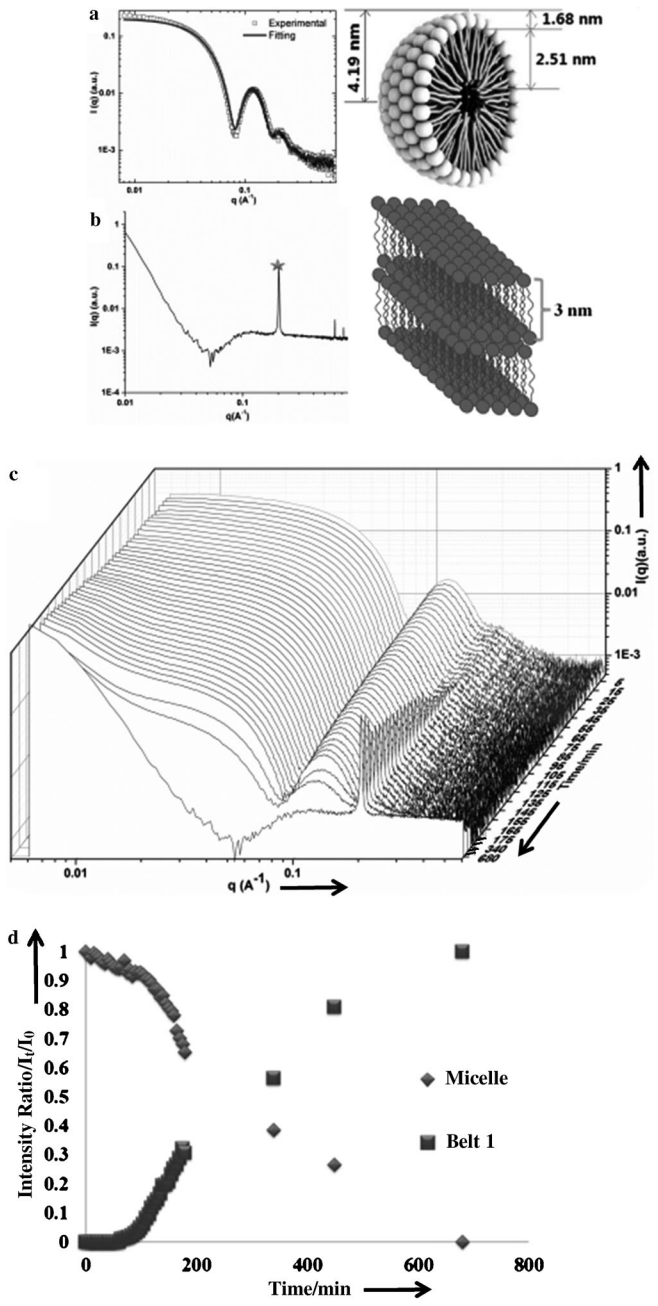

Figure 4. a) Left: SAXS curve of initial solution just after preparation and fitted with core-shell model; right: graphical representation of the micelle structure. b) Left: SAXS curve of solution containing assemblies; right: graphical representation of multilayer structure. c) Time-resolved SAXS results of the solution of the hybrid from 0 to 680 min time. d) Plot of normalized intensities of micelle peak and assemblies peak versus time.

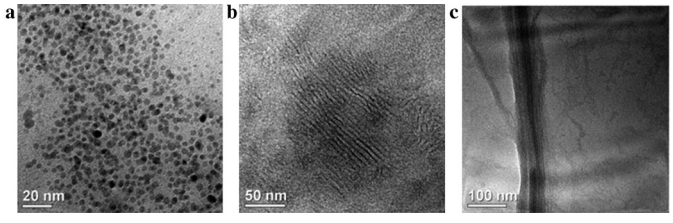

Figure 5. TEM images of a) micelles, b) primary layer phase, and c) growing layer phase structures.

pH of the aqueous solution H_2·**1** was tuned from 13.3 to 7.0 through the addition of extra KOH solution or HCl solution. SEM studies indicate that the belt-like structures can be observed in the solutions with pH range from 13.3 to 9.0, while irregular aggregates without any ordered structures were observed in solutions under conditions of lower pH (Figure 6, and Figures S3 and S4 in Supporting Information). The protonation

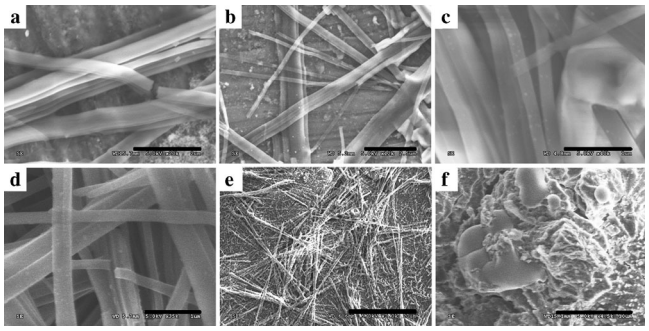

Figure 6. SEM images of the aggregates in solutions of H_2·**1** with a) pH 11.9 (scale bar, 2 μm), b) pH 10.8 (scale bar, 2.5 μm), c) pH 10.5 (scale bar, 1 μm), d) pH 9.8 (scale bar, 1 μm), e) pH 9.0 (scale bar, 20 μm), and f) pH 7.8 (scale bar, 10 μm).

of the two amino groups of the hybrid at low pH could reduce the net charges of the polar head groups as well as the formed micelles. Therefore, the electrostatic interaction between the micelles becomes weaker, while the van der Waals attraction will be dominant. Such a nonspecific interaction (van der Waals attraction) finally leads to the fast coagulation of the micelles to irregular aggregates at low pH. On the other hand, SAXS measurements on the hybrid solutions at the identical pH (~12.6) containing LiOH, NaOH, KOH, or NH_3·H_2O, respectively, show that micelles form in all solutions at the beginning, while nanobelt structures are only eventually observed in KOH and NH_3·H_2O solutions (see supporting information). K^+ and NH_4^+ have smaller hydrated radii among these cations and therefore have stronger affinity with the micelles, leading to easier coagulation of micelles and formation of the nanobelts at higher pH. Suggested by SAXS measurements, spherical micelle structures are stable in solution with Na^+ or Li^+ as the counterions without forming either nanobelt or irregular aggregates in these solutions (see Supporting Information).

The role of directional hydrogen bonding in the formation of 1D nanobelt

It has been confirmed above that the nanobelt structure is due to the binding of cations to the anionic micellar surface, which decreases the stability of the micelles leading to the further coagulation and the growth of large structures. The directional noncovalent interactions are responsible for anisotropic properties of supramolecular assemblies.[8a,14] Cronin et al. investigated the self-assembly of pyrene-containing hybrids into 1D nanofibres on hydrophilic surfaces, revealing that directional

π–π stacking drove the 1D growth of the nanofibres.[8a] Herein, the hydrogen-bond interaction between the polar head groups is believed to be critical for the growth of the nanobelt structures by providing a directional interaction that leads to the 1D anisotropic assemblies. FT-IR studies of the single crystals of TBA_2·**1**, nanobelt structures (prepared in solution at pH ~13.3 and separated as a solid sample through centrifugation), an H_2·**1** sample prepared through ion exchange (see experimental section), and irregular aggregates of the hybrid (prepared and separated in solution at pH ~7.0) indicate that the characteristic peaks of V=O_t vibration are at 943, 945, 952, and 956 cm^{-1}, respectively (see Figure S5 and S6 in Supporting Information). The lower V=O_t vibration frequencies confirm the existence of hydrogen-bond interaction, since the involvement of terminal oxo ligand of the polar head groups in hydrogen bonding slightly elongates the bond length of V=O_t, and consequently lowers the V=O_t vibration frequencies. The first and second samples have orderly packed hybrid structures and show lower vibrational frequencies, implying the critical role of hydrogen bonding in forming 1D-ordered structures. Moreover, proved by the time-resolved SAXS measurements, the formation of nanobelt structures becomes significantly slower when adding 1 M urea or replacing H_2O with D_2O in the KOH solution of the hybrid (lag phase periods >2 days). The plausible explanation is that the added urea or D_2O prefer to interact with the hybrids' polar head groups through hydrogen bonding, which hinders the interhybrid hydrogen bonding. Hydrogen bonds can only form with the specific donor and acceptor positions, which force the growth of the hybrid assemblies to proceed in one specific direction to form 1D nanostructure.

Assemblies works as heterogeneous catalyst

The surface of the nanobelts with nanoscaled thickness is fully covered by catalytically active hexavanadates, making them potential high efficient heterogeneous catalysts. Herein, the catalytic efficiency of nanobelts is evaluated based on the reaction time of catalyzed oxidative desulfurization with hydrogen peroxide. The 1D assemblies are stable in acetonitrile and were used to catalyze the oxidation of methyl *p*-tolylsulfide with two equivalents of H_2O_2 (wt, 30%) (Figure 7a,b, and Supporting Information). The sulfide was fully oxidized into sulfide monoxide and sulfone (molar ratio, 1:1) after running the reaction for 1.5 h at 40 °C with the loading of nanobelts (6.0 mg, Figure 7c). After another three hours, all the sulfide monoxide was finally turned into sulfone (Figure 7c). SEM studies indicate that the belt structures remain after the reaction (Figure S7 in Supporting Information). The catalysts were easily re-collected through centrifugation and further reactions proved that the catalysts did not lose catalytic efficiency for at least two more cycles. Moreover, catalytic reactions with different loading amounts of the heterogeneous catalysts (0–6 mg of nanobelts) and one homogeneous catalyst (TBA_2·**1**, soluble in acetonitrile, 6 mg) were carried out. The time needed for the sulfide to be fully consumed is inversely proportional to the amount of the heterogeneous catalysts (Figure 7d). The reaction goes faster with the homogeneous catalyst (reaction time 40 min), but the heterogeneous catalysis provides both reasonably fast rate (1.5 h) and good recyclability for the catalysts. Due to their high surface area, our heterogeneous catalysts (90 min) show higher reaction rate than the previous Keggin-type POM-based heterogeneous catalyst (150 min).[15]

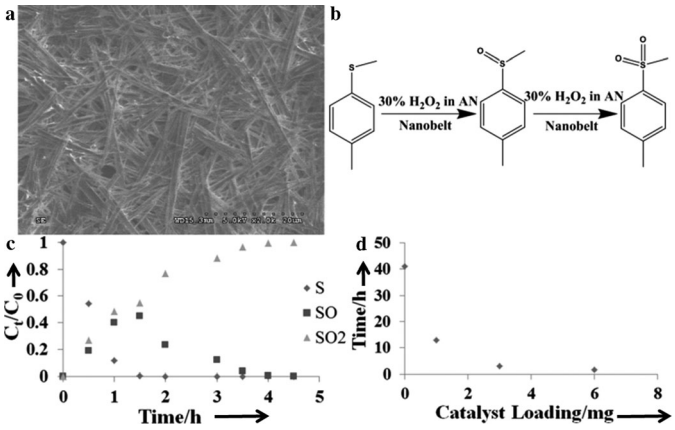

Figure 7. a) SEM image of the assemblies dispersed in acetonitrile after 1 day. b) Reaction scheme for the oxidation of sulfide catalyzed by the assemblies. c) Kinetic curves of the concentrations of reactant and products in the reaction catalyzed by 6 mg nanobelts (S, *p*-tolylsulfide; SO, sulfide monoxide; SO_2, sulfone). d) Reaction time of oxidation of sulfide with different loading amount of nanobelts.

Conclusion

In summary, a new inorganic-organic hybrid surfactant with a hexavanadate cluster as the polar head group was designed, synthesized, and programmed to self-assemble into 1D nanobelt structures. The assembly mechanism was proved to be the coagulation of hybrid micelles into layered structures with the cooperation of hydrophobic, electrostatic, and hydrogen-bonding interactions, while the last one is particularly important as it is directional and leads to the anisotropic assemblies. The assemblies were highly efficient heterogeneous catalysts for oxidation of organic sulfides, because of their nanoscale thickness and the exposure of most of the hexavanadates onto the surface.

Experimental Section

Synthesis of TBA_2·1

A solution of cetyl 4-(chloromethyl)benzoate (0.39 g, 1 mmol) and $[(n\text{-}C_4H_9)_4N]_2[V_6O_{13}\{(OCH_2)_3CNH_2\}_2]$ (1.23 g, 1 mmol) in *N,N*-dimethyl formamide (15 mL) was stirred for 48 h at 80 °C, then cooled to room temperature. A solution of tetrabutyl ammonium hydroxide (1.04 g, 0.8M) in methanol (1.25 mL) was added to the reaction solution and stirred for 30 min at room temperature; the resulting solution was added to deionized water (100 mL) for precipitating. After standing for a few days, the solution was filtered and the precipitate was washed by deionized water three times and then dried in air. The solid was dissolved in acetonitrile and filtered to remove insoluble substance; the filtrate was precipitated by adding diethyl ether and then separated by centrifugation. The

acetonitrile–dissolution–diethyl ether–precipitation procedure was repeated two more times and yield the final product (0.32 g, 20.4%). Single crystals of TBA_2·**1** were afforded by slow diffusion of solution of (TBA_2·**1**) in acetonitrile into deionized water. ^{1}HNMR (400 MHz, [D_6]DMSO): $\delta = 0.85$ (t, $J = 6.7$ Hz, 3H; CH_3, tail), 0.93 (t, $J = 7.3$ Hz, 24H; CH_3, $[Bu_4N]^+$), 1.23 (m, 24H; $(CH_2)_{12}$, tail), 1.30/1.32(m, 16H, CH_2; $[Bu_4N]^+$), 1.57 (m, 16H; CH_2, $[Bu_4N]^+$), 1.69 (m, 2H; $COOCH_2$-CH_2, tail), 3.17 (t, $J = 7.3$ Hz, 16H; NCH_2, $[Bu_4N]^+$), 3.85/3.87 (d, $J = 6.4$ Hz, 2H; $NHCH_2$, tail), 4.23 (t, $J = 6.5$ Hz, 2H; $COOCH_2$, tail), 4.67 (s, 6H, $(OCH_2)_3$, side without tail), 4.87 (s, 6H; $(OCH_2)_3$, side with tail), 7.47/7.49(d, J=8.2 Hz, 2H; CH, phenyl), 7.84/7.86 ppm (d, $J = 8.2$ Hz, 2H; CH, phenyl); IR (KBr pellet): $\tilde{\nu} = 3350$, 3314, 2960, 2926, 2873, 2854, 1720, 1611, 1483, 1469, 1274, 1101, 1087, 1065, 945, 816, 796, 720, 583 cm^{-1}; ESI (MeCN): *m/z*: 554.38 [$\mathbf{1}^{2-}$], 1109.14 [(**1**+H)$^-$], 1350.61 [(**1**+TBA)$^-$]; elemental analysis calcd (%) for $C_{64}H_{126}N_4O_{21}V_6$: C 48.24, H 7.97, N 3.52; found: C 48.48, H 7.92 N 3.44.

Crystal data for TBA_2·1

Formula: $C_{64}H_{126}N_4O_{21}V_6$; $M_r = 1593.33$, triclinic, $P\bar{1}$, $a = 10.690(2)$, $b = 11.537(5)$, $c = 31.412(14)$ Å, $\alpha = 84.74(4)$, $\beta = 82.61(3)$, $\gamma = 89.47(3)^\circ$, $V = 3826(3)$ Å^3, $Z = 2$, $\rho_{calcd} = 1.383$ g cm^{-3}, $\mu = 0.772$ mm^{-1}, $F(000) = 1688.0$, crystal size $= 0.4 \times 0.3 \times 0.1$ mm^3. A total of 30332 reflections were collected, of which 13432 were unique ($R_{int} = 0.0635$). $R_1 = 0.0954$ for 9474 independent reflections with [$I > 2\sigma(I)$], $wR_2 = 0.1737$ for all data. The data were collected at 101(2) K on a Xcalibur E diffractometer with $Mo_{K\alpha}$ monochromated radiation ($\lambda = 0.71073$ Å). The structure was solved by direct methods using SHELXS-97 and refined using SHELXL-97.[3] CCDC-994169 contains the supplementary crystallographic data for this paper. These data can be obtained free of charge from The Cambridge Crystallographic Data Centre via www.ccdc.cam.ac.uk/data_request/cif.

Cation exchange technology for the synthesis of H_2·1

TBA_2·**1** (10 mg) was dissolved in CH_2Cl_2 (ca. 2.5 mL) and commercially available concentrated HCl solution (ca. 0.5 mL) was added. The solutions were put into sonication for 10 min and then centrifugation (speed, 6000 rpm) for 30 min. The red solid sample at the bottom of centrifuge tube was collected and dried in air. FT-IR and ^{1}H NMR measurements of H_2·**1** confirm the removal of TBA cations and the stability of the anion surfactant (see Supporting Information).

Catalytic activity of the assembly structures

tert-Toyl sulfide (130 μL), H_2O_2 (30%, wt; 300 μL), octane (65 μL) and the catalysts, TBA·**1** (homogeneous catalyst, 6 mg) or different loading amount of the nanobelts (heterogeneous catalyst: from 0 to 6 mg), were mixed in acetonitrile (3 mL). The reaction solution was kept at 40 °C by using an oil bath, with stirring at 1000 rpm. GC-MS (Hewlett Packard 5890 Series II) was used to monitor the reactions. Octane was used as standard to measure the relative concentration of reactant and products. Relative concentration of certain species was calculated as $c = (I_t/I_{octane,t})/(I_{sulfide,0}/I_{octane,0})$. The nanobelt catalysts were recycled through centrifugation and washed with acetonitrile.

Acknowledgements

This work is supported by NSF (CHE1305756), Lehigh University, and the University of Akron. This material is based upon work supported as part of the Institute for Atom-efficient Chemical Transformations (IACT), an Energy Frontier Research Center funded by the U.S. Department of Energy, Office of Science, and Office of Basic Energy Sciences. P.Y. acknowledges the department fellowship from chemistry department of Lehigh University and Bob Jagendorf for providing us with the picture of factory. T.L. and R.E.W. are thankful for the use of the Advanced Photon Source, an Office of Science User Facility operated for the U.S. Department of Energy (DOE) and Office of Science by Argonne National Laboratory, supported by the U.S. DOE under Contract No. ED-AC02-06CH11357. Y.W. acknowledges the support of Tsinghua University Initiative Foundation Research Program No. 20101081771 and NSFC (Nos. 21225103 and 21221062) and THSJZ. We thank Dr. Xiaobing Zuo and Dr. Byeongdu Lee for helpful discussions.

Keywords: catalysis · noncovalent interactions · organic–inorganic hybrid · polyoxometalates · self-assembly

[1] a) S. Zhang, D. M. Marini, W. Hwang, S. Santoso, *Curr. Opin. Chem. Biol.* **2002**, *6*, 865–871; b) Y. S. Lee, in *Self-Assembly and Nanotechnology*, Wiley, **2007**, pp. 183–219; c) G. M. Whitesides, B. Grzybowski, *Science* **2002**, *295*, 2418–2421; d) Y. Yan, M. B. Chan-Park, Q. Zhang, *Small* **2007**, *3*, 24–42; e) M. Fujita, in *Structure and Bonding, Vol. 96* (Ed.: D. M. P. Mingos), Springer, Berlin, **2000**, p. 236; f) D. S. Lawrence, T. Jiang, M. Levett, *Chem. Rev.* **1995**, *95*, 2229–2260; g) T. Aida, E. W. Meijer, S. I. Stupp, *Science* **2012**, *335*, 813–817.

[2] a) M. Mastrangeli, S. Abbasi, C. Varel, C. V. Hoof, J.-P. Celis, K. F. Böhringer, *J. Micromech. Microeng.* **2009**, *19*, 083001; b) G. M. Whitesides, M. Boncheva, *Proc. Natl. Acad. Sci. USA* **2002**, *99*, 4769–4774; c) F. Li, D. P. Josephson, A. Stein, *Angew. Chem.* **2011**, *123*, 378–409; *Angew. Chem. Int. Ed.* **2011**, *50*, 360–388.

[3] a) J.-M. Lehn, *Proc. Natl. Acad. Sci. USA* **2002**, *99*, 4763–4768; b) F. M. Menger, *Proc. Natl. Acad. Sci. USA* **2002**, *99*, 4818–4822; c) D. Philp, J. F. Stoddart, *Angew. Chem.* **1996**, *108*, 1242–1286; *Angew. Chem. Int. Ed. Engl.* **1996**, *35*, 1154–1196.

[4] a) A. Mershin, B. Cook, L. Kaiser, S. Zhang, *Nat. Biotechnol.* **2005**, *23*, 1379–1380; b) N. Stephanopoulos, J. H. Ortony, S. I. Stupp, *Acta. Mater.* **2013**, *61*, 912–930; c) B. Soreghan, J. Kosmoski, C. Glabe, *J. Biol. Chem.* **1994**, *269*, 28551–28554; d) P. A. Korevaar, S. J. George, A. J. Markvoort, M. M. Smulders, P. A. Hilbers, A. P. Schenning, T. F. De Greef, E. W. Meijer, *Nature* **2012**, *481*, 492–496.

[5] a) L. Cronin, A. Muller, *Chem. Soc. Rev.* **2012**, *41*, 7333–7334; b) D.-L. Long, R. Tsunashima, L. Cronin, *Angew. Chem.* **2010**, *122*, 1780–1803; *Angew. Chem. Int. Ed.* **2010**, *49*, 1736–1758.

[6] a) M. T. Pope, in *Encyclopedia of Inorganic Chemistry*, Wiley, **2006**; b) P. Yin, D. Li, T. Liu, *Isr. J. Chem.* **2011**, *51*, 191–204.

[7] a) P. Yin, D. Li, T. Liu, *Chem. Soc. Rev.* **2012**, *41*, 7368–7383; b) A. Dolbecq, E. Dumas, C. d. R. Mayer, P. Mialane, *Chem. Rev.* **2010**, *110*, 6009–6048; c) A. Proust, B. Matt, R. Villanneau, G. Guillemot, P. Gouzerh, G. Izzet, *Chem. Soc. Rev.* **2012**, *41*, 7605–7622.

[8] a) M. H. Rosnes, C. Musumeci, C. P. Pradeep, J. S. Mathieson, D.-L. Long, Y.-F. Song, B. Pignataro, R. Cogdell, L. Cronin, *J. Am. Chem. Soc.* **2010**, *132*, 15490–15492; b) Y.-F. Song, R. Tsunashima, *Chem. Soc. Rev.* **2012**, *41*, 7384–7402; c) D.-Y. Du, J.-S. Qin, T.-T. Wang, S.-L. Li, Z.-M. Su, K.-Z. Shao, Y.-Q. Lan, X.-L. Wang, E.-B. Wang, *Chem. Sci.* **2012**, *3*, 705–710; d) Y. Wang, I. A. Weinstock, *Chem. Soc. Rev.* **2012**, *41*, 7479–7496; e) M. A. Alam, Y.-S. Kim, S. Ogawa, A. Tsuda, N. Ishii, T. Aida, *Angew. Chem.* **2008**, *120*, 2100–2103; *Angew. Chem. Int. Ed.* **2008**, *47*, 2070–2073.

[9] a) P. Yin, J. Wang, Z. Xiao, P. Wu, Y. Wei, T. Liu, *Chem. Eur. J.* **2012**, *18*, 9174–9178; b) P. Yin, P. Wu, Z. Xiao, D. Li, E. Bitterlich, J. Zhang, P. Cheng, D. V. Vezenov, T. Liu, Y. Wei, *Angew. Chem.* **2011**, *123*, 2569–2573; *Angew. Chem. Int. Ed.* **2011**, *50*, 2521–2525; c) Q. Chen, D. P. Goshorn, C. P. Scholes, X. L. Tan, J. Zubieta, *J. Am. Chem. Soc.* **1992**, *114*,

4667 – 4681; d) A. Müller, J. Meyer, H. Bögge, A. Stammler, A. Botar, *Z. Allg. Anorg. Chem.* **1995**, *621*, 1818 – 1831.
[10] S. Förster, A. Timmann, M. Konrad, C. Schellbach, A. Meyer, S. S. Funari, P. Mulvaney, R. Knott, *J. Phys. Chem. B* **2005**, *109*, 1347 – 1360.
[11] F. Kremer, W. Richtering, in *Scattering Methods and the Properties of Polymer Materials, Vol. 130* (Eds.: N. Stribeck, B. Smarsly), Springer, Berlin, Heidelberg, New York, **2005**.
[12] V. M. Fokin, N. S. Yuritsyn, E. D. Zanotto, in *Nucleation Theory and Applications*, Wiley-VCH, Weinheim, **2005**, pp. 74 – 125.
[13] a) J. Zhang, D. Li, G. Liu, K. J. Glover, T. Liu, *J. Am. Chem. Soc.* **2009**, *131*, 15152 – 15159; b) I. G. Johnston, A. A. Louis, J. P. K. Doye, *J. Phys. Condens. Matter* **2010**, *22*, 104101.
[14] a) C. M. A. Leenders, L. Albertazzi, T. Mes, M. M. E. Koenigs, A. R. A. Palmans, E. W. Meijer, *Chem. Commun.* **2013**, *49*, 1963 – 1965; b) T. Hirose, F. Helmich, E. W. Meijer, *Angew. Chem.* **2013**, *125*, 322 – 327; *Angew. Chem. Int. Ed.* **2013**, *52*, 304 – 309.
[15] M. Carraro, G. Fiorani, L. Mognon, F. Caneva, M. Gardan, C. Maccato, M. Bonchio, *Chem. Eur. J.* **2012**, *18*, 13195 – 13202.

Received: April 5, 2014
Published online on July 9, 2014